Feasibility of 3D Printing on Environmentally Friendly Cementless Materials with Low Thermal Conductivity

Wei-Ting Lin[1,*], Dariusz Mierzwiński[2], Marek Hebda[2], Andina Sprince[3], Gábor Mucsi[4]

[1]Department of Civil Engineering, National Ilan University, Yilan, Taiwan, ROC

[2]Department of Materials Engineering, Cracow University of Technology, Kraków, Poland

[3]Institute of Civil Engineering, Faculty of Civil and Mechanical Engineering, Riga Technical University, Riga, Latvia

[4]Institute of Raw Material Preparation and Environmental Technology, University of Miskolc, Miskolc, Hungary

Received 14 June 2024; received in revised form 22 November 2024; accepted 25 November 2024

DOI: https://doi.org/10.46604/ijeti.2024.13853

Abstract

This study investigates ultra-fine fly ash (UFA) and co-fired fly ash (CFA) to produce binary cementless binders without alkali activators and determines the effects of molding temperatures (17 ℃, 50 ℃, 60 ℃, 70 ℃, 80 ℃, and 90 ℃) on thermal conductivity and microstructures. The pastes are subjected to flow and expansion tests to verify the mixing state of the two industrial by-products for a fixed water-to-binder ratio of 0.4. Compressive strength, water absorption, density, thermal conductivity, and scanning electron microscope analyses determine material properties and the optimal molding temperature. Results reveal that higher hardening temperatures lead to higher water absorption and lower density. The 50 ℃ specimen exhibits the lowest thermal conductivity of 0.1796 W/m·K at 56 days. The printed specimens with UFA and CFA at a 1:1 ratio achieve a 28-day compressive strength of 9 MPa and a thermal conductivity of 0.2064 W/m·K.

Keywords: 3D printing technology, co-fired fly ash, thermal conductivity, circular economy

1. Introduction

Statistically, approximately 4.1 billion tons of cement are produced annually, accounting for nearly 8% of the total carbon dioxide emissions generated by human activities [1]. To meet the global carbon reduction vision, the large amount of carbon dioxide generated by the construction industry cannot be ignored. In recent years, the recycling of industrial by-products has become one of the leading research directions for cement materials [2]. Cementless materials produced from a mixture of two or more industrial by-products have been proven to replace Portland cement as cementitious materials [3]. Many studies have practically confirmed their safety and resistance to sulfuric acid [4-5]. Regarding their characteristics, the lightweight cementless materials developed by Yum et al. [6] exhibit low density and low thermal conductivity, making them suitable for high-quality applications.

At present, ultra-fine fly ash (UFA) is a novel industrial by-product mainly produced in thermal power plants. Many studies have confirmed that the spherical shape of the particles provided better flow properties when replacing cement, and the smaller particle size compared to conventional fly ash also contributed to higher compressive strength in the manufacture of geopolymers [7-8]. During the 1970s, countries focused on developing new thermal power generation systems in response to the oil crisis. Due to the use of less volatile fuels, the circulation of fluidized bed boilers was accepted and quoted by the

* Corresponding author. E-mail address: wtlin@niu.edu.tw

English language proofreader: Chih-Wei Chang

Taiwanese industry for their environmental performance. It has also begun to be emphasized that co-fired fly ash (CFA) can be reused. Lin et al. [4] found that CFA, with strong alkaline properties, can substitute alkali activators to produce an alkali-free cementless material using a 6:4 ratio of ground-granulated blast-furnace slag and CFA. It achieved a compressive strength of 30 MPa at 28 days and 80% of the strength of cement specimens. The strength sources were C-S-H and C-A-S-H colloids formed by $Ca(OH)_2$, SiO_2, and Al_2O_3.

3D printing technology has been widely used in machining, chemical processes, and daily life. This technology, for instance, enables consumers to print mobile phone cases and phone accessories. However, it has recently been applied to developing 3D concrete printing technology and technical research. It has started to carry out concrete printing projects such as buildings or structural elements [9]. Unfortunately, construction regulations in most countries have not yet been developed to allow building construction through 3D printing [10]. Thinking from the perspective of the construction industry, it is worthwhile to begin by printing non-structural components as a way of promoting and applying this innovative technology. Cementless materials are suitable for printing non-structural components and have sustainability indicators such as low carbon, environmental protection, and material reuse.

Geopolymers or alkali-activated materials as construction materials for 3D printing have also been a focus of research and development in recent years [11]. Therefore, this study developed cementless printable materials without alkali agents and special construction functions with low thermal conductivity. These materials can be used as non-structural components. The development of printable low thermal conductivity materials allows for the use of decorative layers, surface layers, or interlayers for walls or roof panels, which improves the thermal insulation of buildings and reduces energy use and carbon dioxide emissions. The aforementioned printable innovative materials have considerable commercial potential and are highly novel.

Thermal insulation of building materials is indispensable due to the heat island effect in urban areas. Building materials with the most efficient insulation performance provided the most comfortable environmental comfort. This was done by effectively blocking the influence of heat from the external environment of the building on the room temperature, reducing energy consumption. The cement-based materials used in traditional buildings had high thermal conductivity. Thicker types of glass fiber cotton, polystyrene foam, rock wool, rubber foam, and polyurethane foam were used to reduce thermal conductivity. Geopolymers reduce thermal conductivity by using their material properties.

However, developing an appropriate proportion of cementless materials reduced chemicals, and in turn, increased the value of industrial waste reuse, improving thermal conductivity and the thickness of the materials. The insulation performance was inversely proportional to its density and thermal conductivity. Therefore, the density of thermal insulation materials was usually low, and the industry often used lightweight concrete to achieve thermal insulation. Still, its ecological properties were not favorable; hence, scholars have used geopolymers as an alternative material. Due to the low energy consumption and excellent mechanical properties in the manufacture of geopolymer, it was possible to achieve a low thermal conductivity ($<$ 0.70 W/m·K) that was about 50% lower than that of cement-based materials [12].

To achieve higher thermal insulation, foaming agents were incorporated into geopolymers to reduce density and thermal conductivity, and these materials were also called foam geopolymers. According to Łach et al. [13], the thermal conductivity of foam geopolymers with additives was found to be 0.17 W/m·K to 0.08 W/m·K. This study used UFA and CFA as binders to make alkali-free cementless materials. The specimens were examined at different molding temperatures (17 ℃, 50 ℃, 60 ℃, 70 ℃, 80 ℃, and 90 ℃) and were subjected to compression strength, water absorption, density, thermal conductivity tests, and scanning electron microscope (SEM) observations. The purpose of this study is to determine the optimum molding temperature for the material to achieve the lowest thermal conductivity coefficient. Fig. 1 presents the flow chart for the study.

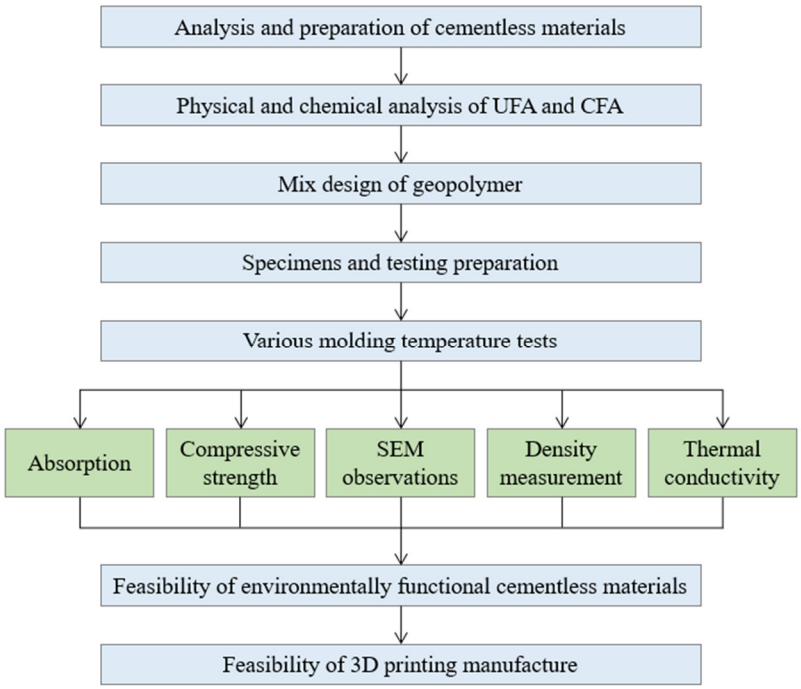

Fig. 1 Creative research methodology for environmentally friendly cementless materials

2. Materials and Methods

This section presented the deployment of two industrial by-products as binders to produce cementless materials using the technology without adding alkali activators. The content includes materials, specimen preparation, and test methods. Prototypes were also made by 3D printing. It indicates that the composites had superior thermal conductivity and that alkali activators were unnecessary for composite formation, where the composites were also highly environmentally friendly.

2.1. Materials

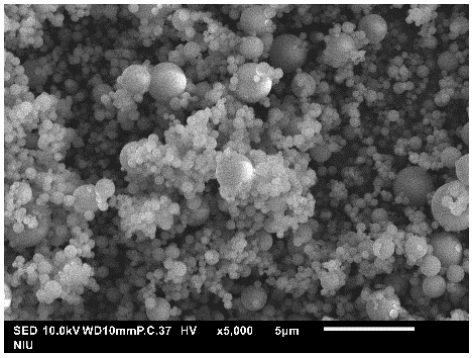

(a) UFA

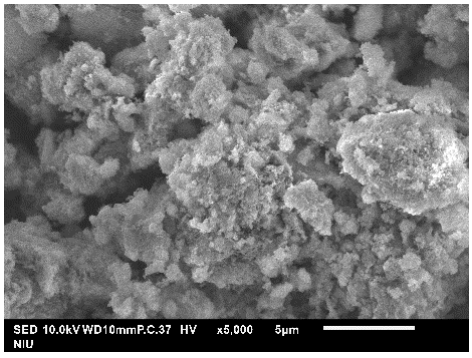

(b) CFA

Fig. 2 SEM photos of the raw materials (5,000x)

Table 1 Chemical compositions of the raw materials

Chemical composition (%)	UFA	CFA
Na_2O	0.93	-
MgO	0.61	1.55
Al_2O_3	17.10	17.58
SiO_2	53.33	22.00
P_2O5	1.08	0.42
SO_3	2.03	11.23
K_2O	2.38	0.41
CaO	10.65	42.13
TiO_2	1.25	0.78
Cr_2O_3	0.01	-
MnO	0.27	0.06
Fe_2O_3	8.94	3.49
ZrO_2	0.06	0.03
Others	1.36	0.34

In this study, the UFA provided by Triaxis Company was used. Specifically, UFA had a particle size of 0.1-10μm, ten times smaller than cement particles, a specific gravity of 2.61, a fineness of 22,400 cm^2/g, and a Pozzolanic activity strength index of 124%. Fig. 2(a) presents an SEM image of UFA, which appeared as spherical particles. The chemical composition of UFA was similar to that of conventional fly ash, but the activity index was higher. CFA was provided by Yuen Foong Yu Paper Mfg. Co., Ltd., with a specific gravity of 2.73, fineness of 2,800 cm^2/g, and Pozzolanic activity strength index of 102%. On the other hand, Fig. 2(b) presents an SEM image of CFA, which was irregularly shaped, and the average particle size of CFA was about 5-10 times larger than that of UFA particles. Besides, the fineness of UFA was significantly higher than that of conventional fly ash (4,000-10,000 cm^2/g) in Taiwan. The results of the XRF tests are described in Table 1.

2.2. Specimen preparation

In this study, the material properties of cementless materials were investigated at different curing temperatures based on the extension of the author's previous experimental results [14]. The cementless materials were synthesized using a blend of UFA and CFA mixed in a 1:1 ratio, and a fixed water-to-binder ratio of 0.4 was used to synthesize the paste specimens. The choice of combining UFA and CFA aimed to achieving an optimal balance between reactivity and internal particle packing, which has been shown to improve the overall mechanical performance of the materials. The experimental procedure followed a controlled curing regime to assess the influence of temperature on the mechanical properties of the prepared specimens.

Firstly, the test specimens were placed in the oven at 50 ℃, 60 ℃, 70 ℃, 80 ℃, and 90 ℃ for 24 hours. Secondly, the specimens were cooled to room temperature, removed from the oven, demolded, and then placed in air at room temperature (17 ℃) for 7 days. The intermediate step was introduced to enable the specimens to stabilize, facilitating the development of a homogenous microstructure before subsequent immersion. Finally, they were immersed in saturated lime water for 28 days. This multi-phase curing methodology was designed to capture the effects of accelerated curing temperatures during the early stages (24 hours) and the stabilization and long-term hydration processes in subsequent stages. The results are anticipated to provide insights into how varying curing temperatures affect key properties such as compressive strength, thermal conductivities, and microstructural development of cementless materials. Furthermore, the findings can contribute to optimizing curing regimes for commercial sustainable binder systems in construction.

2.3. Testing methods

In Table 2, the tests, the dimensions of the specimens, and the standards are listed. First, the density test was conducted by placing the specimen in an air-dry condition. Second, the weight of the specimen was measured. Third, the length, width, and height of the specimen were measured using vernier calipers, with the average taken from 10 locations on each side. Subsequently, the volume was calculated. Finally, the weight of the specimen was divided by its volume to determine its density. The length variation test was conducted by pouring the freshly mixed paste into the mold in two layers. The pastes were pounded 25 times with a pounding rod in the second step. Their volume variation was measured within 7 days after a length-measuring device was placed above them.

Table 2 Testing methods

Test measurement	Specimen dimensions (cm)	Standard	Age (days)
Flowability	-	ASTM C1437	-
Length variation	$\phi 5 \times 10$	-	-
Density	$5 \times 5 \times 5$	-	7
Absorption	$5 \times 5 \times 5$	ASTM C642	28
Thermal coefficient	$\phi 10 \times 5$	-	28, 56
Compressive strength	$5 \times 5 \times 5$	ASTM C109	7, 14, 28
SEM	Fragments	ASTM C1723	28
3D printing for compressive strength	$5 \times 5 \times 5$	ASTM C109	7, 28, 56
3D printing for thermal coefficient	$10 \times 10 \times 5$	-	28

The thermal conductivity test was conducted using a portable thermal conductivity analyzer (ISOMET2114), as shown in Fig. 3. Based on the reference temperature of 23±3 ℃, the thermal conductivity was measured by applying epoxy resin around the air-dried specimen. The average of the three specimens was taken as the result of each test. The study utilized the UM 2205 paste-type 3D printer, which has a maximum printing area of 700 × 600 × 600 mm, a nozzle of 20 mm, and a printing speed of 30 mm/s. The compressive strength test specimens were printed at 5 × 5 × 5 cm, while the thermal conductivity test specimens were printed at 10 × 10 × 5 cm. A total of 7 layers were printed. The appearance of the 3D printer is shown in Fig. 4.

Fig. 3 Appearance of the thermal conductivity analyzer

Fig. 4 Appearance of the 3D printer

3. Results and Discussion

This section discussed the flowability, compressive strength, density, length variation, water absorption, and thermal conductivity of cementless materials. The microscopic behavior of the materials was observed using SEM. The difference in compressive strength between steel molds and 3D-printed specimens was also discussed.

3.1. Flowability

Table 3 shows the average flowability of 64.75% obtained from three tests under the ratio of UFA:CFA of 1:1, which was significantly different from the standard flowability of 110%. The variation between the highest and lowest values is relatively small (1.25%). The data suggested a high level of consistency in the mix proportions, with only minor variations in flowability properties across the specimens. Table 4 shows flow testing results with different proportions of UFA and CFA mixtures.

Table 3 Flowability

Test measurements	NO. 1	NO. 2	NO. 3
Average flow diameter (cm)	16.55	16.45	16.425
Flowability (%)	65.50	64.50	64.25
Avg.	64.75		

Table 4 Flowability of mixing various proportions (%)

Materials	Proportions						
UFA	100%	90%	80%	70%	60%	50%	40%
CFA	0%	10%	20%	30%	40%	50%	60%
Flowability	126.3	79.5	73.8	66.3	66.0	61.3	54.0

In 100% UFA pastes, the flowability reached 126.3%, indicating a significantly high value. The first level of CFA addition (90:10 ratio) caused a sharp drop to 79.5% (a 37% decrease), and each subsequent 10% increase led to a gradual decline from 73.8% to 54.0%. Flowability decreased by 72.3% in descending order. An average decrease of 12% was observed for each 10% variation. Mix proportions and flowability were not perfectly linear, suggesting complex interactions between materials.

It was found that using UFA instead of CFA improved the flowability of cementless materials. Since the fineness of UFA was larger than that of CFA [15], the flowability of UFA with spherical particles was better than that of CFA with irregular particles [14]. It is because the spherical particles minimize interlocking, have lower friction, and reduce the effect of cohesion, thereby exhibiting better fluidity.

3.2. Length variation

Fig. 5 shows the length variation relationship curves for cementless materials, where positive values represent shrinkage. The test was conducted under containment pressure, and the specimen was placed at room temperature. The results showed that the first three hours of the specimen presented significant shrinkage due to the hydration. For initial shrinkage (0-3 hours), all three specimens exhibited rapid initial shrinkage.

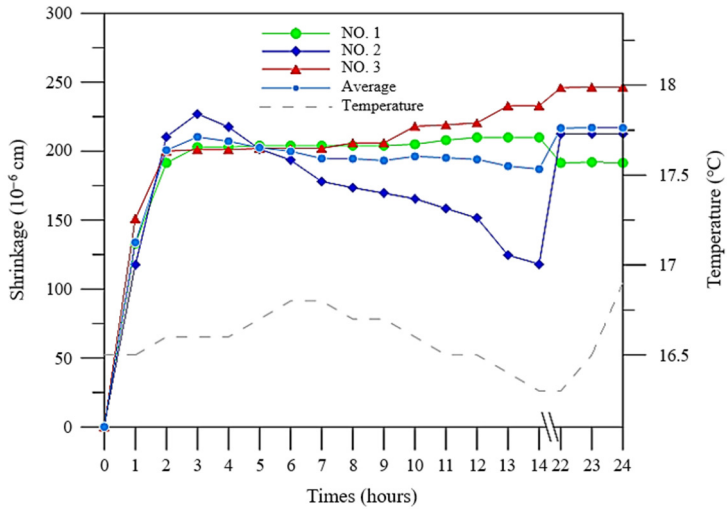

(a) 24-hour length variation

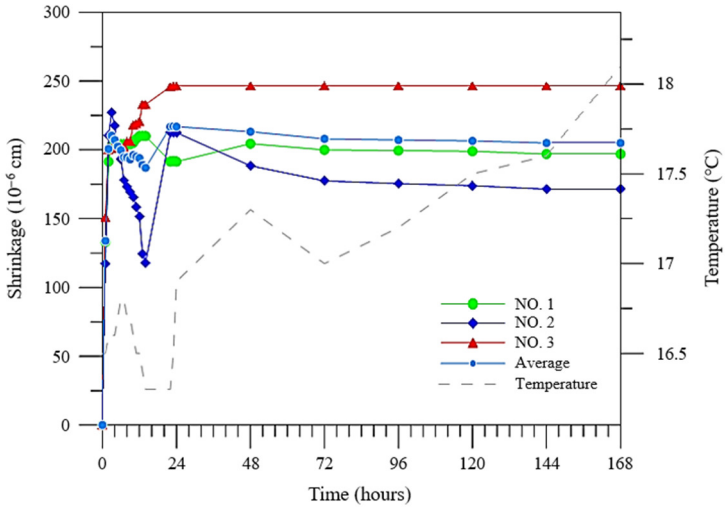

(b) 168-hour length variation

Fig. 5 Drying shrinkage curves

NO. 1 and NO. 3 specimens exhibited nearly identical behavior, reaching approximately 200×10^{-6} cm shrinkage within 2-3 hours. NO. 2 specimens exhibited less shrinkage, reaching approximately 220×10^{-6} cm within 3 hours. Concerning mid-duration shrinkage (3-14 hours), all specimens fluctuated during this period. NO. 1 and NO. 3 specimens showed a gradual decrease in shrinkage, while NO. 2 remained relatively stable at a lower level. Regarding late shrinkage (22-24 hours), both NO. 1 and NO. 3 specimens suddenly increased to approximately 210×10^{-6} cm after a gap in the data. However, NO. 2 showed minimal change, remaining at its previous lower shrinkage level.

Throughout the observed period, NO. 2 consistently exhibited lower shrinkage than NO. 1 and NO. 3. NO. 1 and NO. 3 behaved similarly, with their shrinkage levels closely tracking each other. The final surge in shrinkage for NO. 1 and NO. 3 further reinforced this similarity. The length variation of the cementless material was significant within 48 hours and stabilized after 48 hours, with an average variation of 205 μm for the three specimens. Overall, shrinkage increased rapidly within the initial hours and stabilized over time, with temperature remaining relatively constant. The shrinkage was greater than the expansion at room temperature (17±1 ℃). The study indicated that the specimen shrank due to the evaporation of aluminosilicate colloids [16].

3.3. Density

Fig. 6(a) presents the histograms of the density of the reactive ultra-fine fly ash and co-fired fly ash (RUFA-CFA) cementless specimens. It demonstrated the relationship between temperature and density, with values ranging from 1.31 to 1.40 g/cm^3 across temperatures from 17.5 to 90 ℃. The graph shows how density varied with temperature, generally increasing at 50 ℃ followed by a slight decrease as the temperature rose further. The highest density was observed at 50 ℃ (1.40 g/cm^3), while the lowest values were at the highest temperatures (1.31 g/cm^3 at both 80 and 90 ℃). Due to the high-temperature molding of the specimens, the sulfide in CFA was affected by the high temperature to form calcium alumina or ettringite, thereby resulting in volume expansion and fine cracks [12]. Therefore, it can be concluded that the specimen temperature is directly proportional to the volume expansion and inversely proportional to the density herein. Fig. 6(b) shows that the specimen expanded and protruded from the square mold after hardening. Generally, cementless materials with a density of less than 1.80 are classified as lightweight materials [17].

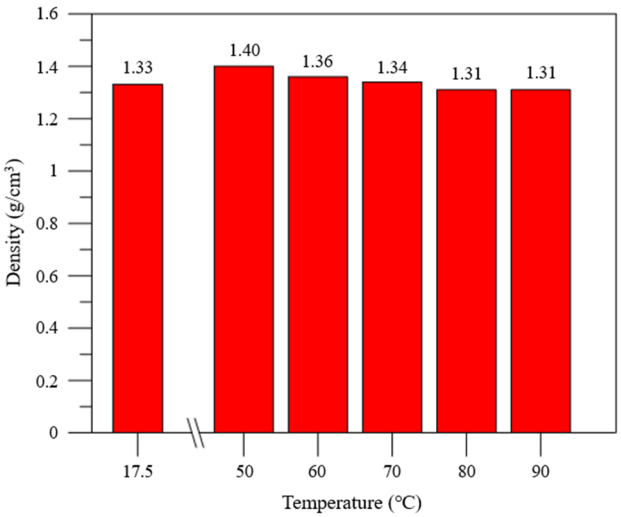

(a) Histograms of measured densities

(b) High temperature (80 ℃) caused the expansion

Fig. 6 Density test compilation diagram

3.4. Absorption

Fig. 7 presents histograms of the absorption of the RUFA-CFA cementless specimens. The volume of the specimen increased with the increase in the hardening temperature, which also caused larger pores and water absorption in the specimens. The absorption (37-39%) significantly exceeded that of ordinary cement-based composites containing supplementary cementitious materials (8-10%) [4]. The pore size distribution of foaming cement-based materials also significantly affected water absorption.

According to the theory of capillary transport, the smaller the pore size, the stronger the capillary force and the greater the water absorption capacity. However, extremely small pore sizes may restrict the movement of water molecules, resulting in a slower water absorption process [18]. Therefore, an optimal pore size range balanced the water absorption with the water

absorption capacity. Kearsley and Wainwright [19] found that the highest water absorption of 30-40% was found when the average pore size of foaming cement-based materials was in the range of 50-200 μm. With this deduction, the pore size of the cementless material ranged from 50-200 μm. This pore size range was ideal for water absorption, enabling efficient absorption without compromising material strength.

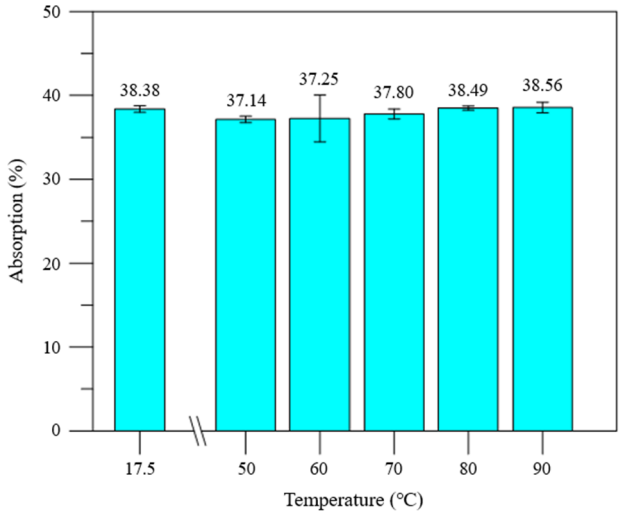

Fig. 7 Histograms of measured absorption

3.5. *Thermal coefficient*

Fig. 8 presents histograms of the thermal coefficient of the RUFA-CFA cementless specimens, and the specimens were measured in air-dry conditions. The thermal conductivity of the specimens ranged from 0.27-0.33 W/m·K at 28 days, whereas it decreased to 0.17-0.22 W/m·K at 56 days. The thermal conductivity of the specimens was significantly lower than that of cement-based materials (1.60-2.50 W/m·K). The low thermal conductivity materials developed in this study were produced without foaming agents, and it is hypothesized that the UFA-CFA paste underwent foaming due to the micro-expansion effect caused by the hydration heat process of the fine particles derived from UFA. This foaming mechanism is analogous to previous studies, where silica fume and chemicals produced a similar foaming effect [20].

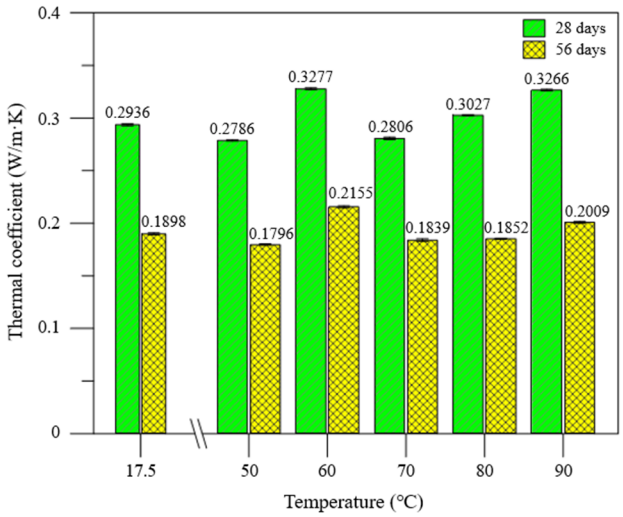

Fig. 8 Histograms of measured thermal coefficient

The cementless materials developed in this study were compared with foamed materials described in previous studies (including foam pastes or foamed concrete). The low thermal conductivity and high water absorption of the material were due to its porous properties [21]. Increasing the porosity of foamed materials significantly impacted their thermal conductivity. For instance, when the porosity of foamed cement was increased from 20 to 70%, its thermal conductivity decreased from 0.40

W/m·K to approximately 0.15 W/m·K [22]. This drop in thermal conductivity was attributed to the decrease in the solid framework of the material resulting from high porosity, which reduced the thermal conductive paths. Similarly, considering every 10% increase in porosity, the thermal conductivity of foamed cement was lowered by about 0.05-0.10 W/m·K [23].

Pore size distribution is also a significant factor affecting the thermal conductivity of foamed materials. When the average pore size of foamed cement-based materials was reduced from 149 to 202 μm, the thermal conductivity ranged from as low as 0.16 W/m·K, and the water absorption rate was higher than 40% [24]. Another study pointed out that the average pore size of foamed materials ranged between 80 to 90 μm, with the corresponding thermal conductivity between 0.26 to 0.28 W/m·K [25]. The thermal conductivity of the cementless materials developed in this study was around 0.20 W/m·K, indicating that the average pore size was less than 200 μm, which is consistent with the results of the aforementioned water absorption. Furthermore, the cementless materials developed in this study exhibited excellent thermal insulating properties, making them suitable for applications such as thermal insulators and insulation.

3.6. Compressive strength and SEM observations

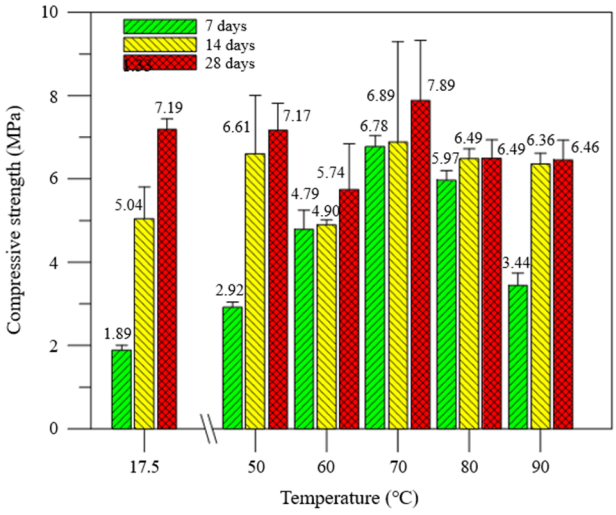

Fig. 9 Histograms of measured compressive strength

Fig. 9 presents the compressive strength of the UFA-CFA cementless specimens. Overall, the compressive strength of 14 days reached more than 70% of that of 28 days, and the strength of the later period was higher than 5 MPa. The specimens with higher molding temperatures accelerated the hydration reaction, enabling the compressive strength at 14 days to exceed 85% of that at 28 days. The strength of the heat-hardened specimens was similar to that of the room-temperature-hardened specimens (28 days to 7.19 MPa). The compressive strength of the cementless specimens was similar to that of lightweight cement mortar or concrete (between 2 MPa and 20 MPa) [26].

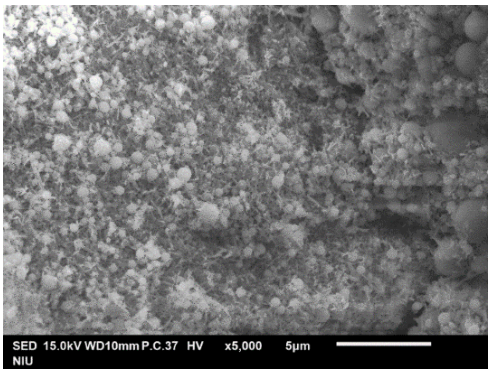

(a) Room-temperature specimen

Fig. 10 SEM photos of the cementless materials (5,000x)

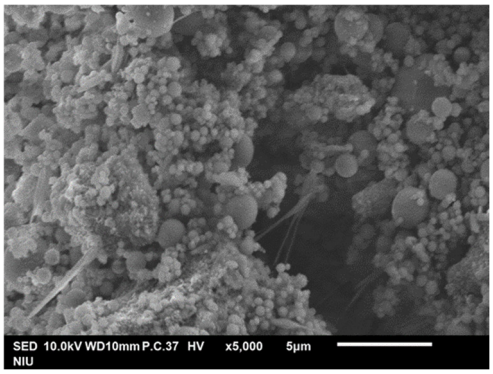

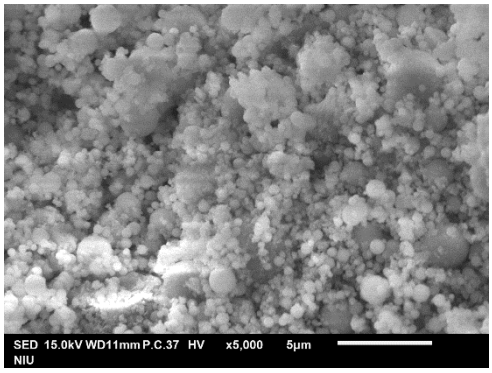

(b) 90 ℃ specimen (c) 70 ℃ specimen

Fig. 10 SEM photos of the cementless materials (5,000x) (continued)

Fig. 10 illustrates SEM micrographs of the specimen hardened at room temperature and the specimen hardened at a heated temperature (70 ℃ and 90 ℃). The cracks in the 90 ℃ specimen were found in ettringite (needle-like crystals) and were more significant than those in the room-temperature specimen due to volume expansion induced by ettringite formation [27]. In addition, ettringite and unreacted UFA can be observed in the room-temperature specimen, which was interlocked and stacked to form a porous structure. Such a microporous structure provided a material efficiency that reduced thermal conductivity. It should also be noted that the porous structure only exhibited a compressive strength of 5-10 MPa. SEM photos of the 70 ℃ specimens revealed that hydration reactants were observed between the interstitial gaps between the two raw materials. A more significant number of tiny pores was also clearly observed. The 70 ℃ specimens had smaller pores, resulting in slightly higher thermal conductivity than others.

3.7. Efficacy of 3D printing specimens

Fig. 11 presents the development curves of compressive strength of cementless specimens with different manufacturing processes. The w/b of the cementless specimens was modified to 0.47 according to actual practice to meet the printer's printability requirements. Printed specimens were cured at room temperature for 7, 28, and 56 days for compressive strength testing. The remaining paste after printing was filled into steel molds to produce molded specimens for strength comparison. The appearance of the printed specimen is shown in Fig. 12, where the axial and lateral compressive forces are marked.

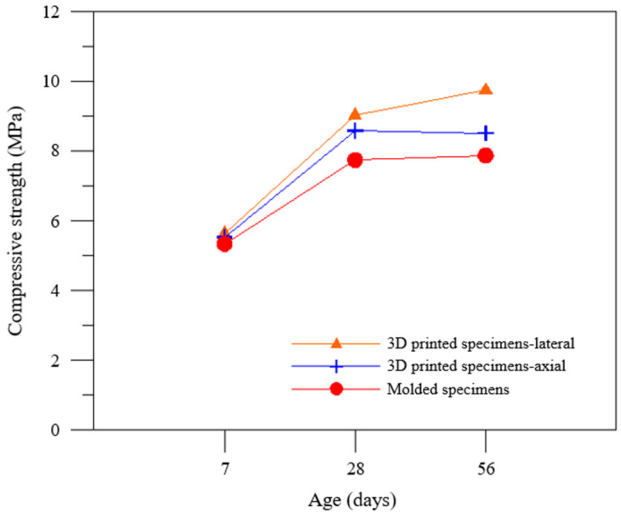

Fig. 11 Compressive strength curves for different processes

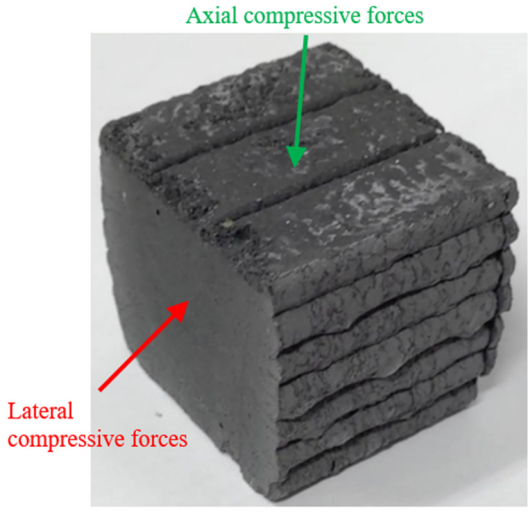

Fig. 12 Appearance of printed specimen

The results revealed that the compressive strength of the printed specimens was superior to that of the molded specimens. The lateral compressive strength in the printed specimens was superior to the axial compressive strength. The irregularity in the contact surface caused by the printing path reduced the intensity of the axially pressurized surface. The lateral compressive

strengths were 5.63 MPa, 9.03 MPa, and 9.74 MPa at 7, 28, and 56 days, respectively. The initial size of the printed specimen was 25 × 5 × 5 cm, and it was cut to 5 × 5 × 5 cm after 30 minutes of rest following production. The cut surface was the lateral compressive surface, as shown in Fig. 11. The section was a smooth surface, and there were no obvious air bubbles or pores in the section of the printed specimen. The thermal conductivity of the 3D printed specimens at 28 days was 0.2064 W/m·K, while that of the molded specimens was 0.1898 W/m·K.

The molded specimens possessed lower thermal conductivity. From the previous description, it is clear that thermal conductivity decreased as the average pore size diminished. The better compressive strength of the printed specimens indicated that the specimens manufactured by this printing technique achieved better compactness, which was reflected in a slightly higher thermal conductivity in the same proportion. The printing technique produced cementless materials with the desired thermal conductivity and mechanical properties. It was also used to produce materials with exceptional thermal conductivity and compressive strength. This cementless with low-thermal-conductive materials provided comparable results to other foamed geopolymer materials [28-30]. It also had the benefit of being printable.

4. Conclusions

This study aimed to develop cementless materials with low thermal conductivity without the use of chemical agents. The materials provided green and renewable properties such as low carbon emissions, economical cost, recyclability, and met sustainable development goals. The main conclusions are summarized as follows:

(1) The cementless materials produced at high temperatures were lightweight (minimum density ≈ 1.31 g/cm^3) and exhibited low thermal conductivity without the use of foaming agents.
(2) The 28-day compressive strength of cementless materials reached up to 7.89 MPa.
(3) The UFA-CFA-produced cementless material demonstrated a minimum thermal conductivity of 0.1796 W/m·K.
(4) The properties of room-temperature-hardened specimens were similar to those of heated-hardened specimens.

A heating hardening process was found to be detrimental to the thermal conductivity and lightweight properties of cementless materials, resulting in redundant energy waste. Moreover, the compressive strength of the 3D printed specimens was better than that of the molded specimens and demonstrated excellent printing behavior. The maximum compressive strength of the printed specimens (at 56 days) reached 9.74 MPa, while the thermal conductivity coefficient was maintained at 0.2064 W/m·K. The low thermal conductivity cementless material developed in this study is well-suited for future applications of 3D printing technology in engineering practice.

Acknowledgments

This research was funded by the National Science and Technology Council of Taiwan (NSTC) under NSTC-111-2923-E-197-003-MY3.

Conflicts of Interest

The authors declare no conflict of interest.

References

[1] L. Poudyal and K. Adhikari, “Environmental Sustainability in Cement Industry: An Integrated Approach for Green and Economical Cement Production,” Resources, Environment and Sustainability, vol. 4, article no. 100024, 2021.
[2] X. Zhang, C. Bai, Y. Qiao, X. Wang, D. Jia, H. Li, et al., “Porous Geopolymer Composites: A Review,” Composites Part A: Applied Science and Manufacturing, vol. 150, article no. 106629, 2021.

[3] T. M. Do, G. O. Kang, and Y. S. Kim, "Development of a New Cementless Binder for Controlled Low Strength Material (CLSM) Using Entirely By-Products," Construction and Building Materials, vol. 206, pp. 576-589, 2019.
[4] W. T. Lin, K. L. Lin, K. Korniejenko, L. Fiala, A. Cheng, and J. Chen, "Composite Properties of Non-Cement Blended Fiber Composites Without Alkali Activator," Materials, vol. 13, no. 6, article no. 1443, 2020.
[5] W. Zhang, H. Choi, T. Sagawa, and Y. Hama, "Compressive Strength Development and Durability of an Environmental Load-Reduction Material Manufactured Using Circulating Fluidized Bed Ash and Blast-Furnace Slag," Construction and Building Materials, vol. 146, pp. 102-113, 2017.
[6] W. S. Yum, J. Yu, D. Jeon, H. Song, S. Sim, D. H. Kim, et al., "Mechanical and Durability Properties of Cementless Concretes Made Using Three Types of CaO-Activated GGBFS Binders," Materials, vol. 15, no. 1, article no. 271, 2022.
[7] W. T. Lin, "Reactive Ultra-Fine Fly Ash as an Additive for Cement-Based Materials," Materials Today Communications, vol. 25, article no. 101466, 2020.
[8] W. T. Lin, K. L. Lin, K. Korniejenko, and L. Fiala, "Comparative Analysis Between Fly Ash Geopolymer and Reactive Ultra-Fine Fly Ash Geopolymer," International Journal of Engineering and Technology Innovation, vol. 11, no. 3, pp. 161-170, 2021.
[9] H. Zhao, Y. Wang, X. Liu, X. Wang, Z. Chen, Z. Lei, et al., "Review on Solid Wastes Incorporated Cementitious Material Using 3D Concrete Printing Technology," Case Studies in Construction Materials, vol. 21, article no. e03676, 2024.
[10] A. Hasani and S. Dorafshan, "Transforming Construction? Evaluation of the State of Structural 3D Concrete Printing in Research and Practice," Construction and Building Materials, vol. 438, article no. 137027, 2024.
[11] A. Yousaf, A. Al Rashid, and M. Koç, "3D Printing of Alkali-Activated Geopolymers for Sustainable and Circular Economy Advancements," Circular Economy, vol. 3, no. 3, article no. 100101, 2024.
[12] R. T. Fongang, J. Pemndje, P. N. Lemougna, U. C. Melo, C. P. Nanseu, B. Nait-Ali, et al., "Cleaner Production of the Lightweight Insulating Composites: Microstructure, Pore Network and Thermal Conductivity," Energy and Buildings, vol. 107, pp. 113-122, 2015.
[13] M. Łach, K. Plawecka, A. Bak, K. Lichocka, K. Korniejenko, A. Cheng, et al., "Determination of the Influence of Hydraulic Additives on the Foaming Process and Stability of the Produced Geopolymer Foams," Materials, vol. 14, no. 17, article no. 5090, 2021.
[14] W. T. Lin, "Development of Cementless Binder for Low Thermal Conductivity Materials: Reactive Ultra-Fine Fly Ash Mixed with Co-Fired Fly Ash," Case Studies in Construction Materials, vol. 16, article no. e00899, 2022.
[15] P. K. De Maeijer, B. Craeye, R. Snellings, H. Kazemi-Kamyab, M. Loots, K. Janssens, et al., "Effect of Ultra-Fine Fly Ash on Concrete Performance and Durability," Construction and Building Materials, vol. 263, article no. 120493, 2020.
[16] C. R. Shearer, J. L. Provis, S. A. Bernal, and K. E. Kurtis, "Alkali-Activation Potential of Biomass-Coal Co-Fired Fly Ash," Cement and Concrete Composites, vol. 73, pp. 62-74, 2016.
[17] V. Corinaldesi, A. Mazzoli, and R. Siddique, "Characterization of Lightweight Mortars Containing Wood Processing By-Products Waste," Construction and Building Materials, vol. 123, pp. 281-289, 2016.
[18] J. Dang, X. Tang, J. Xiao, and A. Han, "Influence of Alkaline Activator and Precursor on the Foam Characterization and Alkali-Activated Foamed Concrete Properties," Cement and Concrete Composites, vol. 145, article no. 105341, 2024.
[19] E. P. Kearsley and P. J. Wainwright, "Porosity and Permeability of Foamed Concrete," Cement and Concrete Research, vol. 31, no. 5, pp. 805-812, 2001.
[20] S. Shakouri, Ö. Bayer, and S. T. Erdoğan, "Development of Silica Fume-Based Geopolymer Foams," Construction and Building Materials, vol. 260, article no. 120442, 2020.
[21] T. Li, F. Huang, J. Zhu, J. Tang, and J. Liu, "Effect of Foaming Gas and Cement Type on the Thermal Conductivity of Foamed Concrete," Construction and Building Materials, vol. 231, article no. 117197, 2020.
[22] W. She, Y. Chen, Y. Zhang, and M. R. Jones, "Characterization and Simulation of Microstructure and Thermal Properties of Foamed Concrete," Construction and Building Materials, vol. 47, pp. 1278-1291, 2013.
[23] S. Feng, Y. Gao, H. Xiao, and C. Xue, "Influence of Fibers and Bubble Structure on Thermal Conductivity and Mechanical Performances of Foam Concrete," Construction and Building Materials, vol. 445, article no. 137956, 2024.
[24] H. Yuan, Z. Ge, R. Sun, X. Xu, Y. Lu, Y. Ling, et al., "Drying Shrinkage, Durability and Microstructure of Foamed Concrete Containing High Volume Lime Mud-Fly Ash," Construction and Building Materials, vol. 327, article no. 126990, 2022.
[25] D. Chen, M. Chen, Y. Zhang, X. Yang, J. Zhang, Y. Zhao, et al., "Development of an Environmental Foamed Concrete Incorporating Recycled Cement Concrete Powder with Carbonation," Construction and Building Materials, vol. 422, article no. 135833, 2024.

[26] Y. Wu, J. Y. Wang, P. J. M. Monteiro, and M. H. Zhang, "Development of Ultra-Lightweight Cement Composites with Low Thermal Conductivity and High Specific Strength for Energy Efficient Buildings," Construction and Building Materials, vol. 87, pp. 100-112, 2015.

[27] J. Wang, M. Feng, T. Ma, Y. Zhang, and Y. Wang, "The Effects of Desulfurized Gypsum on the Mechanical Properties of Dredged Clay with High Initial Water Content Stabilized by Ternary Geopolymer," Case Studies in Construction Materials, vol. 20, article no. e02907, 2024.

[28] K. Korniejenko, K. Pławecka, P. Bazan, B. Figiela, B. Kozub, K. Mróz, et al., "Green Building Materials for Circular Economy - Geopolymer Foams," Proceedings of Engineering and Technology Innovation, vol. 25, pp. 26-34, 2023.

[29] M. Łach, J. Mikuła, W. T. Lin, P. Bazan, B. Figiela, and K. Korniejenko, "Development and Characterization of Thermal Insulation Geopolymer Foams Based on Fly Ash," Proceedings of Engineering and Technology Innovation, vol. 16, pp. 23-29, 2020.

[30] M. Łach, A. Bąk, K. Pławecka, and M. Hebdowska-Krupa, "Possibility of Using a Geopolymer Containing Phase Change Materials as a Sprayed Insulating Coating - Preliminary Results," Emerging Science Innovation, vol. 2, pp. 01-08, 2024.